Computation of the Asymmetric Vortex Pattern for Bodies of Revolution

J. E. Graham* and W. L. Hankey†
Air Force Wright Aeronautical Laboratories, Wright-Patterson Air Force Base, Ohio

The three-dimensional flowfield surrounding a slender body of revolution at angle of attack was solved through numerical integration of the complete Navier-Stokes equations. The leeside vortex pattern was computed for two separate sets of conditions. First, a flowfield containing laterally symmetric vortices was computed for a three-caliber ogive cylinder at Mach number 1.98 and angle of attack of 20 deg. Second, a flowfield containing laterally asymmetric vortices was computed for a cone cylinder at Mach number 1.6 and angle of attack of 30 deg. Both cases used a laminar flow assumption. All results were obtained on a CRAY-1 computer utilizing MacCormack's algorithm as vectorized by Shang. The computed results compared favorably with the two sets of experimental data used, in that all the primary flow features were captured.

Nomenclature

d	= diameter of body
e	= specific internal energy, $C_v T + (u^2+v^2+w^2)/2$
E,F,G	= vector fluxes
L	= length of body (in the x direction)
n	= outward normal from body surface
p	= static pressure
$\dot{q}$	= rate of heat transfer
R	= radius of the body
Re	= Reynolds number based on body length, $\rho_\infty u_\infty x/\mu_\infty$
t	= time
T	= static temperature
u,v,w	= velocity components in the Cartesian frame
U	= dependent variables in vector form (ρ, ρu, ρv, ρw, ρe)
V	= velocity vector ($u\hat{i}+v\hat{j}+w\hat{k}$)
x,y,z	= coordinates in the Cartesian frame
α	= angle of attack
ξ,η,ζ	= transformed coordinate system
ρ	= density
θ	= circumferential angle around body
$\underline{\underline{\tau}}$	= stress tensor

Subscripts

$\underline{(\ )}$	= tensor

Introduction

NUMEROUS experimental studies[1-12] on slender bodies at high angle of attack have identified the existence of complex flow phenomena. At small to moderate angles of attack (<30 deg) a pair of stationary, laterally symmetric vortices appear on the leeward side (Fig. 1a) as compared with several pairs of asymmetrical vortices for higher angles of attack (30 deg<α<60 deg) (Fig. 1b). These vortices are generally stationary, although intermittent regions of unsteadiness have been observed.[7] The steady, asymmetric case is of considerable interest to the aircraft industry since the large side forces encountered at zero yaw angles are capable of producing aircraft spin. Although this phenomenon has been known to exist for several decades, no reliable analytic prediction method exists. Previous analytic and experimental efforts use the so-called impulse flow analogy[8,9] which emphasized the effect of cross-flow Mach number of the flow development. Woolard[10] analytically verified observations by Chapman et al.[11] that the occurrence of vortex asymmetry onset for circular cones is due mainly to a hydrodynamic instability phenomenon rather than to laterally asymmetric viscous separation. Peake and Tobak[12] noted that the asymmetry in the flow may be related to the stability of the velocity profiles in the vicinity of the singular saddle point that exists in the stream above the body (Fig. 2). They theorized that flow perturbations will affect the saddle point flow so as to trigger the instability mechanism. In fact, this instability mechanism acts in a similar manner as a diffuser switch[13] in fluidics. The instability mechanism triggers the flow to one of the bistable asymmetric conditions much the same as the control ports trigger the asymmetric flow in a 15 deg angle diffuser to one of its bistable conditions. This instability is generally thought to arise from imperfections at the tip of the body. As Coe et al.[14] have indicated, symmetrically placed strakes near the tip can eliminate the asymmetry.

These efforts have aided in the understanding of this physical phenomenon, as have various computational efforts[15,16] in the past. However, it was believed that the numerical solution of the full three-dimensional Navier-Stokes equations is necessary to adequately model the viscous nature of the flow. The practicality of solving these equations has evolved concurrently with the advent of vector processors (CRAY, STAR, ILLIAC). Using a previously developed vectorized Navier-Stokes code[17] a program was initiated to compute the entire flowfield over slender bodies at angle of attack. The first part of this research effort[18] addressed only the symmetric laminar case at 20 deg angle of attack with a lateral symmetry assumption. This paper investigates two additional phases. First, a 360 deg mesh is used to compute the laminar case presented in Ref. 18 without the assumption of lateral symmetry. Second, a cone-cylinder flowfield is computed with laminar flow assumption at 30 deg angle of attack with a Reynolds number of 0.4×10^6 based on a body length of 11.25 cm. In this case an essentially asymmetric leeside flow pattern was produced. We attempt to show that for higher angles of attack (i.e., $\geq$30 deg) the symmetric pattern is "dynamically unstable"[19] when undergoing a perturbation induced by a subtle bias introduced in the numerical algorithm. Verification is given that as shown by other investigations[7,11] this asymmetric pattern is less sensitive to subsequent perturbations.

Presented as Paper 82-0023 at the AIAA 20th Aerospace Sciences Meeting, Orlando, Fla., Jan. 11-14, 1982; submitted Jan. 20, 1982; revision received Jan. 31, 1983. This paper is declared a work of the U.S. Government and therefore is in the public domain.

*Mathematician.
†Senior Scientist. Member AIAA.

Method of Solution

A body-oriented coordinate transformation (technique discussed in Ref. 18) is utilized to map the x,y,z physical space (Fig. 3) into a unit cube in the ξ,η,ζ transformed space. The grid for the ogive cylinder is presented in Ref. 18.

The three-dimensional, compressible Navier-Stokes equations in conservative form are[17]

$$\frac{\partial U}{\partial t}+\frac{\partial E}{\partial x}+\frac{\partial F}{\partial y}+\frac{\partial G}{\partial z}=0$$

where the flux vectors (E,F,G) are specified in Ref. 18.

The transformed equations become

$$\frac{\partial U}{\partial t}+\xi_x\frac{\partial E}{\partial \xi}+\left(\eta_x\frac{\partial E}{\partial \eta}+\eta_y\frac{\partial F}{\partial \eta}+\eta_z\frac{\partial G}{\partial \eta}\right)+\left(\zeta_y\frac{\partial F}{\partial \zeta}+\zeta_z\frac{\partial G}{\partial \zeta}\right)=0$$

The explicit finite difference method of MacCormack[20] as vectorized for the CRAY computer by Shang[17] was employed to obtain a steady-state solution through integration in time from specified initial conditions. The method is second-order accurate throughout, but is conditionally stable subject to a CFL time step restriction.

Boundary Conditions

Ogive Cylinder at 20 deg Angle of Attack

Boundary conditions must be prescribed on the six faces of the cube in the transformed space (Fig. 4). The boundary conditions are the same as outlined in Ref. 18 except for the overlapping region of the physical mesh. Far-field conditions are as follows:

$\alpha=20$ deg	$U_\infty=529$ m/s
$u=U_\infty\cos\alpha$	$T_\infty=177.85$ K
$v=U_\infty\sin\alpha$	$P_\infty=1.722$ kN/m^2
$w=0$	$M_\infty=1.98$

The inflow boundary values were fixed over the span of a computational run, and were derived from a locally conical approximation based on previous results. Hence, flowfield values from the adjacent planar cross section, one spatial step downstream from the previous run, are implemented as a Dirichlet condition at the inflow boundary.

On the leeside of the body, two radial lines are overlapped and all dependent variables are equivalenced along the two radial lines. This condition is represented by

$$U_1=U_{KL-1} \qquad U_2=U_{KL}$$

where KL represents the last point in the angular sweep direction (K direction, $KL=60$).

Initial conditions were derived from the converged solution obtained in Ref. 18 (the 180 deg mesh case) by reflecting the solution about the y axis. Total mesh size was $15\times30\times60$.

Cone Cylinder at 30 deg Angle of Attack

Boundary conditions for the cone cylinder are equivalent to the ones prescribed for the ogive cylinder except for the far-field conditions, specified as follows:

$\alpha=30$ deg	$U_\infty=443$ m/s
$u=U_\infty\cos\alpha$	$T_\infty=274.15$ K
$v=U_\infty\sin\alpha$	$P_\infty=2.075$ kN/m^2
$w=0$	$M_\infty=1.6$

However, a shock exit condition was required in the region of the outer boundary where the bow shock was reflecting on

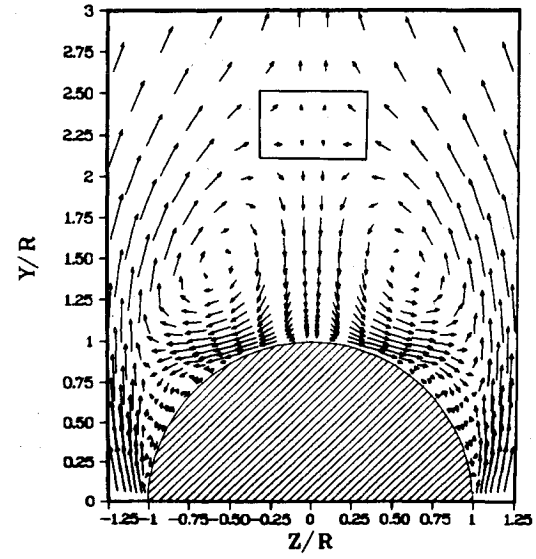

Fig. 2 Illustration of singular saddle point ($\alpha=20$ deg, $M_\infty=1.98$, $x/D=5.8$).

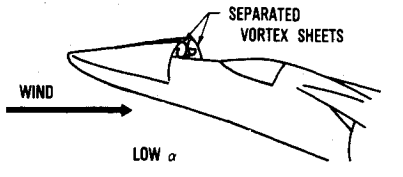

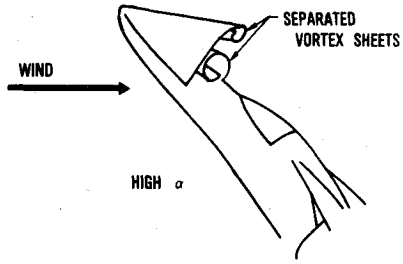

Fig. 1 Flow phenomena.

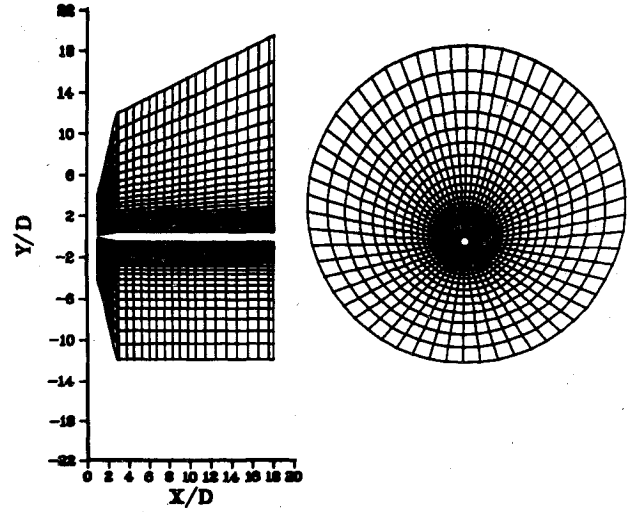

Fig. 3 Physical grid for cone cylinder.

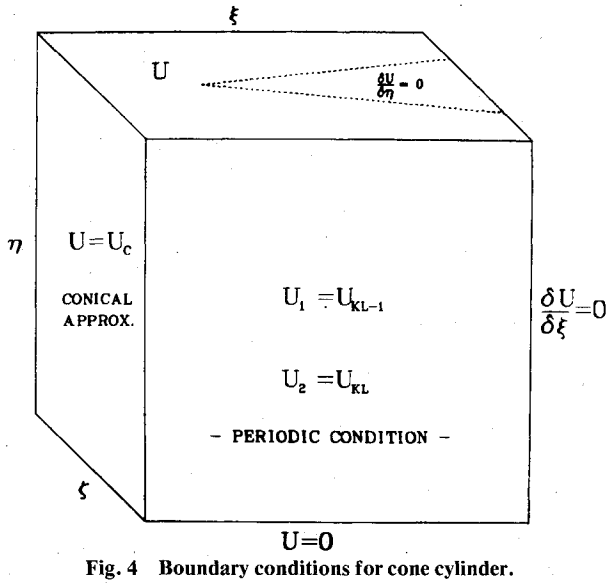

Fig. 4 Boundary conditions for cone cylinder.

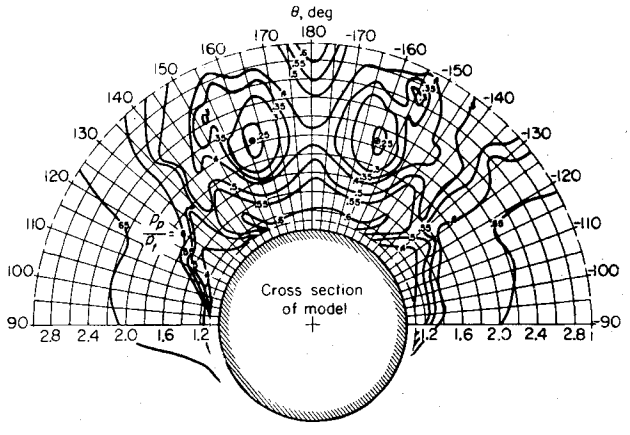

Fig. 5 Pitot pressure survey, $x/D = 10.0$ (Ref. 8).

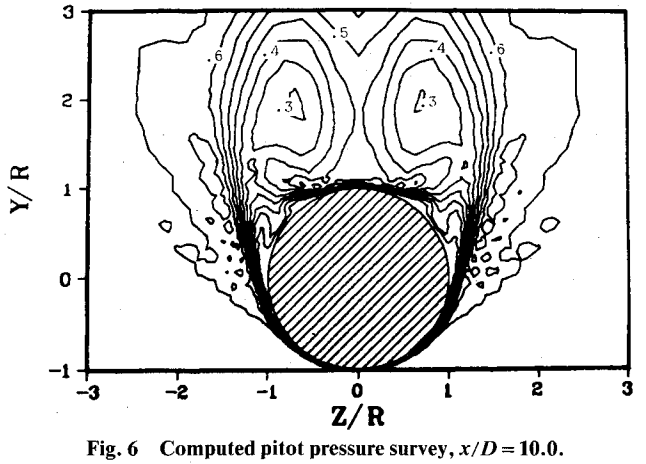

Fig. 6 Computed pitot pressure survey, $x/D = 10.0$.

the leeside of the body (note the dotted line region in Fig. 4). The bow shock was calculated to lie along an angle of 72 deg on the leeside of the body, using the classical Taylor-Maccoll exact solution for flow past a cone. The Neumann condition $\partial U/\partial \eta = 0$ was implemented using first-order differencing within the dotted line area of Fig. 4 in order to allow disturbances induced by reflections of the shock wave to exit the computational domain without adversely affecting the development of the vortex structure near the body.

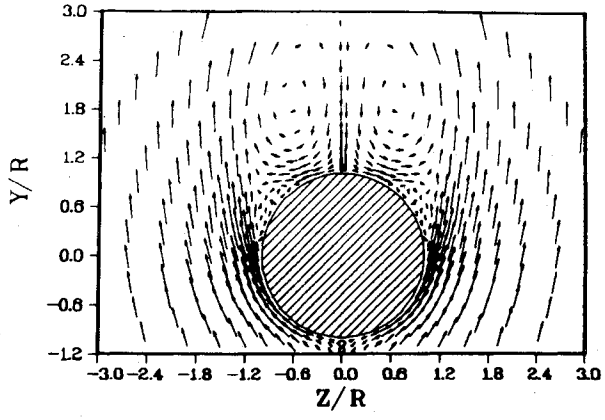

Fig. 7 Computed velocity vectors, $x/D = 10.0$.

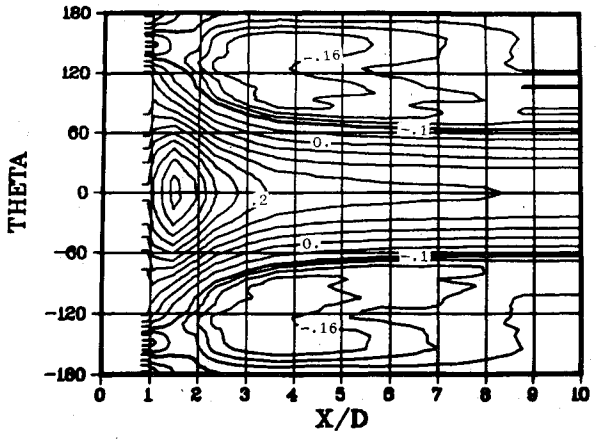

Fig. 8 Computed wall static pressure distribution.

Initial conditions were obtained by rotating all velocity vectors computed in the 20 deg angle of attack case an additional 10 deg from the previously converged solution. The overlapping region of the mesh was located on the windward side of the body for the 30 deg case along the y axis. Total mesh size for this case was $26 \times 30 \times 60$. The additional planes in the x direction were required in order to capture the data reported in the second test of Thomson and Morrison.[7] All boundary conditions were chosen to model the second case in Ref. 7 for comparison purposes.

Numerical Results

Ogive Cylinder at 20 deg Angle of Attack

The case computed was a three-caliber ogive cylinder with a total length of 10 diameters at 20 deg angle of attack. The Mach number was 1.98 and the Reynolds number based on the diameter ($d = 0.9375$ cm) of the cylinder was 0.44×10^6. This set of conditions matches the wind tunnel data of Jorgensen and Perkins[2] for which a pair of symmetric vortices was observed. Experimental data displayed for this case was obtained from figures included in Ref. 2.

Results obtained for this case were essentially the same as displayed in Ref. 18. An indication of the degree of agreement between the experimental and numerical pitot pressure at $x/D = 10.0$ is shown in Figs. 5 and 6. Figure 7 presents the velocity vector field for the same x station, while Fig. 8 shows the symmetric nature of the wall static pressure over the entire 360 deg computation. Hence, it was evident that even with a 360 deg mesh in physical space where no assumption of lateral symmetry is made (as it was in Ref. 18), two symmetric vortices showing very strong agreement with the Jorgensen and Perkins experiment are obtained computationally.

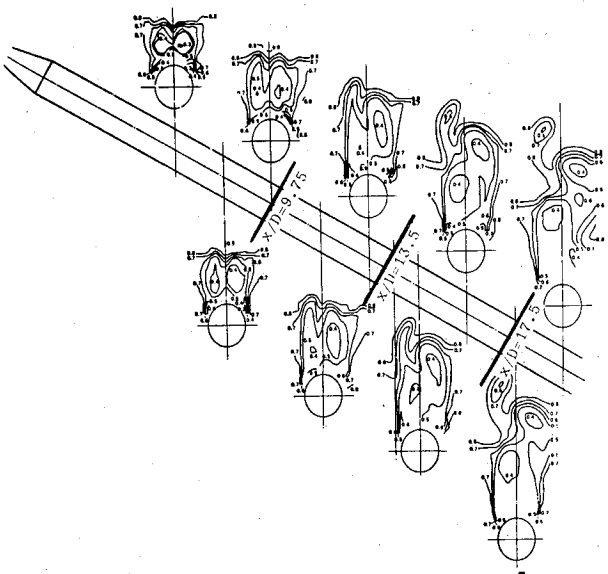

Fig. 9 Experimental pitot pressure surveys.[7]

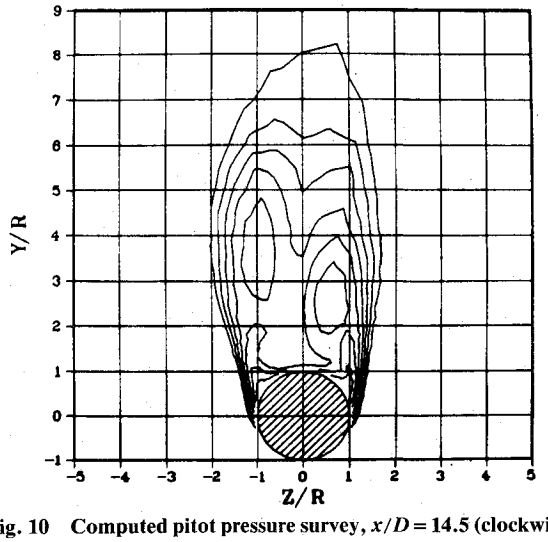

Fig. 10 Computed pitot pressure survey, $x/D = 14.5$ (clockwise).

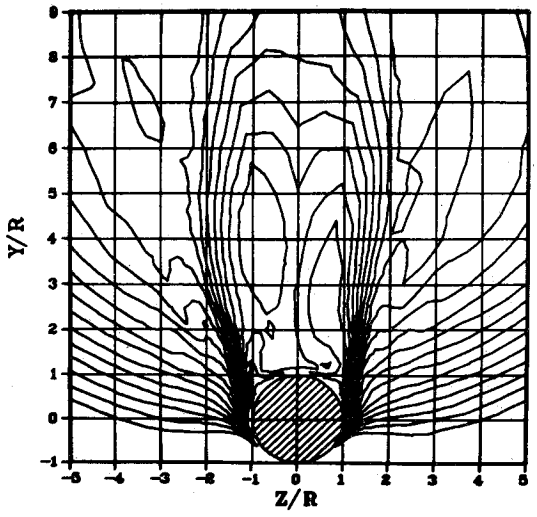

Fig. 11 Computed pitot pressure survey, $x/D = 17.5$ (clockwise).

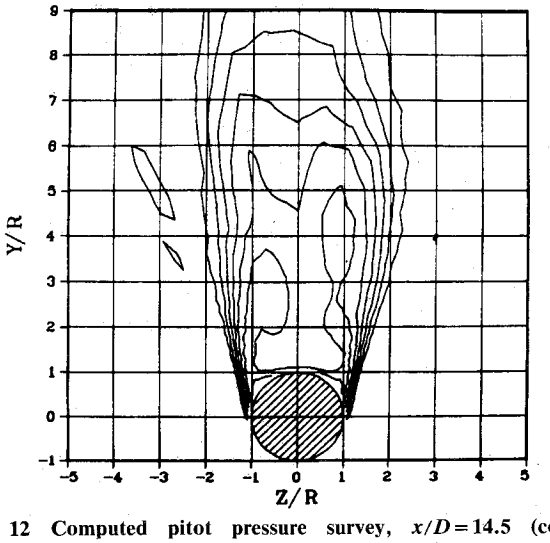

Fig. 12 Computed pitot pressure survey, $x/D = 14.5$ (counterclockwise).

Cone Cylinder at 30 deg Angle of Attack

The second case computed was the flowfield over a cone cylinder with a cone length of 3 diameters and a total length of 18 diameters at 30 deg angle of attack. The Mach number and the Reynolds number based on a body length of 11.25 cm was 0.4×10^6. This set of conditions nearly duplicates the wind tunnel data of Thomson and Morrison.[7] Figure 9 illustrates the results obtained experimentally in terms of pitot pressure surveys in planes taken normal to the freestream direction. Although it is difficult to trace the location of distinct vortices through this series of surveys, the asymmetric nature of the leeside flow pattern is obvious, especially toward the rear of the body ($x/D = 18$).

The asymmetric nature of the flowfield was obtained computationally with a laminar flow assumption, which was quite surprising as transition to turbulence initially was thought to be an important aspect of the problem. Hence, it was thought that a small perturbation, which can be induced by the truncation error produced in the sweep operators of the finite difference algorithm, was amplified to the point of a clear asymmetry downstream from the tip of the cone. This small perturbation, although also present in the 360 deg ogive cylinder case, did not produce any observable flow asymmetry in the corresponding computational domain ($0 \leq x/D \leq 10$). It was assumed that the symmetric flow pattern was dynamically unstable when undergoing a small perturbation. Hence, it was felt that a change in sweep direction could also reverse the pattern of asymmetry on the leeside of the body. A change in sweep direction was achieved by actually leaving the computational code (i.e., differencing sequence) unchanged and transposing the aerodynamic data input to the program so that the algorithm sweeps in the opposite physical direction inside the internal loops (i.e., instead of sweeping from $I = 1$, IMAX we reverse our array in the angular array index to sweep from $I = I\text{MAX}, 1, -1$).

Figures 10 and 11 illustrate the pattern of the flowfield when a clockwise sweep in the angular direction is employed. The location of the two primary vortices is not laterally symmetric. The location of the vortex on the left is displaced further from the body than the vortex on the right. This pattern was reflected about the y axis when the sweep direction was reversed (Figs. 12 and 13). Just how the sweep direction physically triggered the asymmetry is unclear. However, it is believed that it caused an asymmetric separation of fluid from the body downstream, which, in turn, disturbed the singular saddle point shown in Fig. 2. In fact, Singh[21] found that potential theory indicates that as a pair of vortices gets farther from a cylinder (i.e., $y/r > 1.209$), the bistable asymmetric pattern becomes stable once formed. Hence, downstream from the tip of the body the asymmetric pattern is expected to be stable.

The local side force encountered for both sweep directions (Fig. 14) showed the reversal of the pattern of asymmetry was evident although it was disturbing that even though the nature

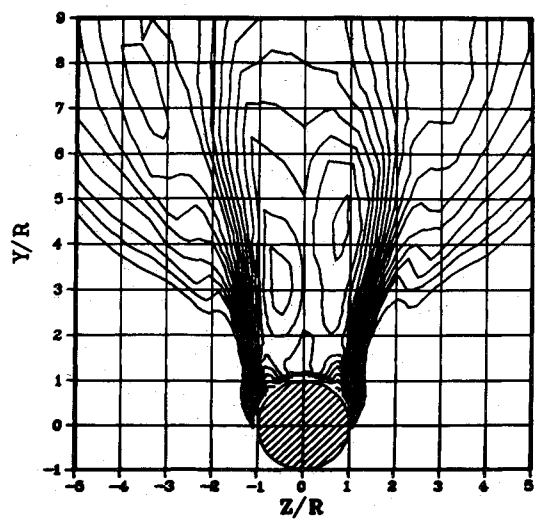

Fig. 13 Computed pitot pressure survey, $x/D = 17.5$ (counterclockwise).

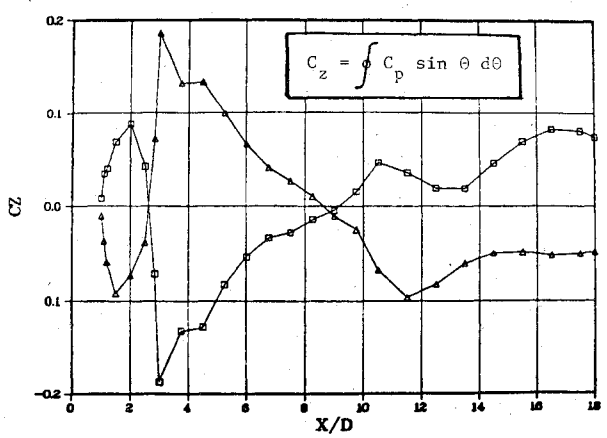

Fig. 14 Local side force coefficient vs axial location (□ —clockwise, Δ—counterclockwise).

of the flow was clearly asymmetric, the magnitude of the computed side force was not as large as would be expected for such a flowfield (see Ref. 14). The grid may have been too coarse near the body to resolve the side force encountered under such circumstances. Additional stretching of the mesh in the radial direction for this case, which was necessary to resolve the bow shock sufficiently, caused the mesh to become slightly less dense near the body on the leeside than for the 20 deg angle-of-attack case.

It should be noted that the computer time required for each case from an initial symmetric condition obtained from the 20 deg angle-of-attack case was approximately 1 h on the CRAY-1 (i.e., for a given sweep direction in case 2).

Conclusion

The aerodynamic forces on slender bodies at high angle of attack depend largely upon the development of the vortex pattern on the leeside. Potential theory is not capable of uniquely determining these forces since viscous forces are essential to the process. Previous investigations have shed light on various aspects of vortex formation, but to correctly compute the viscous phenomenon, the three-dimensional Navier-Stokes equations are required. Without the use of a large-scale vector processor such as the CRAY-1, flowfield simulation of the present magnitude cannot practically be undertaken without limiting the scope of the investigation.

The numerical results showed good agreement with wind tunnel data, especially for the ogive cylinder case ($\alpha = 20$ deg). The cone cylinder case ($\alpha = 30$ deg) showed an asymmetric nature in the computation although discrepancies between numerical and wind tunnel results occurred. Computation results indicated the nature of the asymmetry was dependent upon the algorithm's sweep direction, as the pattern was reflected about the y axis for opposite sweep directions. Hence, a very small perturbation can be induced by finite difference algorithm truncation error which can trigger a hydrodynamic instability above the body. This instability amplifies and causes the flowfield to converge to a point of clear asymmetry downstream from the cone tip. In other words, the switching phenomenon was produced by a numerical bias which is physically amplified to generate the asymmetry. It was interesting to note that all results obtained were steady, even though the time-dependent Navier-Stokes equations were used. This seemed to verify the observation of steady vortex locations on the leeside of the configuration.

References

[1] Fidler, J. E., "Approximate Method for Estimating Wake Vortex Strength," *AIAA Journal*, Vol. 12, May 1974, pp. 633-635.

[2] Jorgensen, L. H. and Perkins, E. W., "Investigations of Some Wake and Vortex Characteristics of an Inclined Ogive-Cylinder Body at Mach Number 2," NACA Rept. 1371, 1958.

[3] Tinling, B. E. and Allen, C. Q., "An Investigation of the Normal Force and Vortex-Wake Characteristics of an Inclined Ogive-Cylinder Body at Subsonic Speeds," NASA TN D-1297, 1962.

[4] Calarese, W., "An Experimental Study of Vortex Flow in the Wake of a Slender Body of Revolution at Large Incidence," AFWAL-TM-80-69-FIMM, May 1980.

[5] Lamont, P. J., "Pressure Measurements on an Ogive-Cylinder at High Angles of Attack with Laminar, Transitional, or Turbulent Separation," AIAA Paper 80-1556, Aug. 1980.

[6] Shivinada, T. P. and Oberkampf, W. L., "Prediction of the Compressible Vortex Wake for Bodies at High Incidence," AIAA Paper 81-0360, St. Louis, Mo., Jan. 1981.

[7] Thomson, K. D. and Morrison, D. F., "The Spacing, Position and Strength of Viscosity on Flow Over Slender Inclined Bodies of Revolution," *Journal of Fluid Mechanics*, Vol. 50, Pt. 4, 1971, pp. 751-783.

[8] Allen, H. J. and Perkins, E. W., "A Study of the Effects of Viscosity on Flow Over Slender Inclined Bodies of Revolution," NACA Rept. 1048, 1951.

[9] Sarpkaya, T., "Separated Flow About Lifting Bodies and Impulsive Flow About Cylinders," *AIAA Journal*, Vol. 4, March 1966, pp. 414-420.

[10] Woolard, H. W., "Similarity Relation for Vortex Onset on Slender Pointed Forebodies," AFWAL-TM-81-77-FIGC, April 1981.

[11] Chapman, G. T., Kenner, E. R., and Malcolm, G. N., "Asymmetric Forces on Aircraft Forebodies at High Angles of Attack—Some Design Guides," Stall/Spin Problems on Military Aircraft, North Atlantic Treaty Organization, AGARD CP 199, Nov. 1975, Ref. 12.

[12] Peake, D. J. and Tobak, M., "Three-Dimensional Interactions and Vortical Flows with Emphasis on High Speeds," AGARD-AG-252, July 1980.

[13] Foster, K. and Parker, G. A., *FLUIDICS: Components and Curcuits*, John Wiley & Sons Ltd., London, 1970, pp. 27-29.

[14] Coe, P., Chambers, J., and Letko, W., "Asymmetric Lateral-Directional Characteristics of Pointed Bodies of Revolution at High Angles of Attack," NASA TN D-7095, 1972.

[15] Rakich, J. V., Vigneron, Y. C., and Agarwal, R., "Computation of Supersonic Viscous Flows Over Ogive-Cylinder at Angle of Attack," AIAA Paper 79-0131, New Orleans, La., Jan. 1979.

[16] Pulliam, T. H. and Steger, J. L., "On Implicit Finite-Difference Simulations of Three-Dimensional Flow," AIAA Paper 78-10, Huntsville, Ala., Jan. 1978.

[17] Shang, J. S., "Numerical Simulation of Wing Fuselage Interference," AIAA Paper 81-0048, St. Louis, Mo., Jan. 1981.

[18] Graham, J. E., Hankey, W. L., and Shang, J. S., "Navier-Stokes Solution of a Slender Body of Revolution at Large Incidence," *AIAA Journal*, Vol. 20, June 1982, pp. 776-781.

[19] Perkins, C. D. and Hage, R. E., *Airplane Performance Stability and Control*, John Wiley & Sons, Inc., New York, 1949, pp. 4-6.

[20] MacCormack, R. W., "The Effect of Viscosity in Hypervelocity Impact Cratering," AIAA Paper 69-354, Cincinnati, Ohio, April-May 1969.

[21] Singh, S. N., "Stability of a Pair of Stationary Vortices in the Leeward Side of a Cylinder in a Potential Flowfield," AFWAL-TR-83-3067, to be published.